Review

Protein-Based Strategies for Non-Alkali Metal-Ion Batteries

Qian Wang , Chenxu Wang * , Wei-Hong Zhong *

Posted Date: 22 July 2025

doi: 10.20944/preprints202507.1731.v1

Keywords: protein; electrochemical; energy storage; batteries; non-alkali metal

Review

Protein-Based Strategies for Non-Alkali Metal-Ion Batteries

Qian Wang [1], Chenxu Wang [2,*] and Wei-Hong Zhong [2,*]

[1] Department of Mechanical Engineering, The University of Texas at Dallas, Richardson, Texas 75080, USA

[2] School of Mechanical and Materials Engineering, Washington State University, Pullman, WA 99164, USA

* Correspondence: chenxu.wang@wsu.edu (C.W.); katie_zhong@wsu.edu (W.-H.Z.)

Abstract

Batteries are a cornerstone of modern technology that support a wide range of applications including portable electronics, electric vehicles and large-scale energy storage for renewable power systems. Despite the widespread use, commercial Li-ion batteries are limited by mineral resources of Li. The rapidly growing battery market demands for alternative battery systems, such as non-alkali metal-ion batteries, that are capable of delivering comparative energy densities. In the meantime, to improve the performance of the batteries via generating sustainable strategies has been broadly studied. Proteins being naturally evolved macromolecules that possess diverse structures and functional groups have been demonstrated to be able to transport various metallic ions inside the bio-organisms. Therefore, active studies have been carried out on the use of natural proteins (e.g., zein, soy, fibroin, bovine serum albumin, etc.) to enhance the electrochemical performance of non-alkali metal-ion batteries. This review provides a comprehensive summary of recent advances on studies of protein-based strategies for non-alkali metal-ion batteries and outlines perspectives for future sustainable electrochemical energy storage systems.

Keywords: protein; electrochemical; energy storage; batteries; non-alkali metal

Contents

 doi:10.20944/preprints202507.1731.v1

1. Introduction

Global energy demand has increased significantly due to rapid industrial growth and electric device development in the past 30 years. Renewable energy sources, such as solar, wind and hydropower, have become key global strategies to address the environmental impact and resource limitations of fossil fuels[1]. The widespread implementation of renewable energy has significantly reduced greenhouse gas emissions generated from conventional thermal power plants. However, the intermittent and seasonal supply of solar and wind energy leads to fluctuating power output, bringing a critical challenge of grid stability and reliability. To address this issue, various energy storage systems have been applied to temporarily store the electric energy produced from renewable energy plants[2]. Among the energy storage systems, rechargeable batteries offer a practical and scalable solution for storing excess energy during periods of surplus generation and delivering it during peak demand effectively. Currently, the widely used batteries are Li-ion batteries, which dominate the market of consumer electronics and electric vehicles due to their high energy density and long cycle life[3]. However, the limitation of Li mineral resources restricts their future sustainable application in large-scale and stationary energy storage systems.

In recent years, significant research has been directed toward the development of alternative battery systems that rely on non-alkali metal-ion batteries, such as Zn-ion batteries[4], Zn-air batteries[5], redox flow batteries[6], bio batteries[7] and so on, have emerged as promising candidates for next-generation grid-scale energy storage. These batteries possess combined advantages of affordability, environmental safety, aqueous electrolyte compatibility and potential for long cycle life[8]. Despite these advantages, challenges such as limited power output, low energy density or capacity degradation still hinder their practical deployment[9]. To address these challenges, the use of specific natural biomaterials has garnered increasing attention based on their natural characteristics[10–12]. Proteins are naturally abundant macromolecules composed of different amino acids with different spatial molecular structures that offer a unique set of properties, making them suitable for various functions in electrochemical systems[13]. For example, protein molecules are rich in nitrogen-containing groups, which can serve as active sites for catalysis or doping sources in carbon materials[14]. Moreover, protein molecules exhibit metal-binding affinities, hydrogen bonding capabilities and structural flexibility that can be used in the design of electrode materials, binders, electrolytes and catalysts[15–17].

In this review, we summarize recent advances in the application of protein-based and protein-derived materials in non-alkali metal-ion batteries for improving their electrochemical performance and environmentally benign behavior **(Figure 1)**. Specifically, we categorize the applications of

 doi:10.20944/preprints202507.1731.v1

protein materials into several sections based on different battery components and battery systems. In the second section, we summarized the reported applications of protein-derived biomass carbon and protein-modified active materials in non-alkali metal-ion batteries including Zn-air batteries and vanadium redox flow batteries. In the third and fourth sections, protein-derived film for stabilizing Zn metal anodes and protein-based hydrogels and gel polymer electrolytes for high-performance Zn-ion batteries were introduced. Protein-based and protein-derived catalysts in bioelectrochemical systems (e.g., biochemical microbial fuel cells and biochemical H_2-NH_3 systems) and polypeptide organic radical active materials were summarized in the fifth and sixth sections. In the last section, the conclusion and perspectives of protein applications in non-alkali metal-ion batteries were summarized.

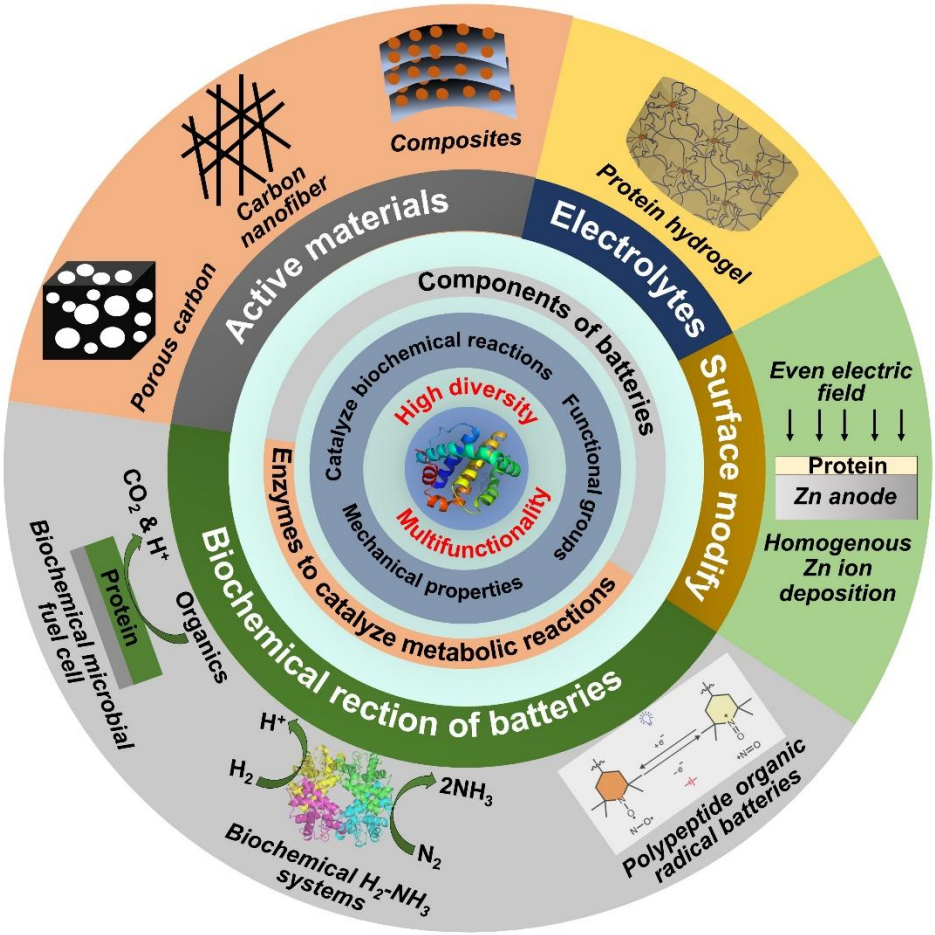

Figure 1. Schematic of protein-based strategies for non-alkali metal-ion batteries.

2. Protein-Derived Materials for Electrodes

2.1. Protein-Derived Carbon

Biomass carbon has emerged as a popular material as the anode in batteries owing to its multifunctionality resulting from its diverse morphology and chemical composition. Specifically, biomass carbon with mesoporous structure offers several advantages, including a large specific surface area that facilitates high electrical conductivity, ionic transfer channels and good wetting with the electrolyte[18,19]. Consequently, biomass carbons with high specific surface area hold great promise as electrode materials for low-cost non-alkali metal-ion batteries. Through changing the parameter of different activation processes and using different raw biomaterials, biomass carbon can be tailored to exhibit tunable pore sizes and chemical constituents, making them suitable for use as conductive matrices for electrodes in non-alkali metal-ion batteries such as Zn-air batteries, fuel cell and vanadium redox flow batteries (Table 1).

 doi:10.20944/preprints202507.1731.v1

Table 1. Protein-derived biomass carbon as the electrodes for non-alkali metal-ion batteries [20–25].

Silk	Defect-rich and N-doped carbon	Zn-air	Voltage gap = 1.39 V, voltaic efficiency = 41.3% after 100 cycles	6.0 M KOH + 0.2 M ZnAC, PVA aqueous gel	Zn	[20]
Root nodule	Fe, Mo, S, N self-doped porous carbon	Zn-air	Half-wave potentials are 0.723 V (vs. RHE) in 0.1 M $HClO_4$ and 0.868 V and 0.1 M KOH solution	6 M KOH + 0.2 M $Zn(CH_3CO_2)_2$	Zn	[21]
		Fuel cell	Flow rate of H_2 was 10 mL min^{-1}, 17.6 mW cm^{-2} with an open-circuit voltage of 0.966 V	H_2 | air	Graphite	
Silk	Carbon fabrics	All-vanadium redox flow batteries	Energy efficiency = 86.8%	1.6 M $VOSO_4$ in 4 M H_2SO_4 solution	Symmetrical	[22]
Twin cocoon	Self-standing monolithic carbon	All-vanadium redox flow batteries	50% redox potential decrease & 192% diffusion slope increase	1.0 M $VOSO_4$ + 3.0 M H_2SO_4	Pt, Ag/AgCl	[23]
Pyroprotein	Carbon felts@ pyroprotein	All-vanadium redox flow batteries	ΔE_p = 0.17 V, energy efficiency = 90% at 40 mA cm^{-2}	0.1 M $VOSO_4$ in 2 M H_2SO_4	Three electrodes	[24]
Zein	Zein-coated carbon black	All-vanadium redox flow batteries	Energy efficiency =85.2% after 100th cycles	Positive: 2 M $VOSO_4$ in 3 M H_2SO_4 Negative: 2 M $VOSO_4$ in 3 M H_2SO_4	Symmetrical	[25]
Protein type	**Carbon type**	**system type**	**Electrochemical performance**	**Electrolyte**	**Counter Electrode**	**Reference**

Note: Symmetrical indicates that both electrodes are the same electrode.

2.1.1. Protein-Derived Carbon for Electrodes of Zn-Air Batteries

Silk protein has been utilized as a precursor to synthesize porous nitrogen-doped nanocarbon (SilkNC/KB) featuring abundant structural defects, which was subsequently employed as electrocatalysts for the oxygen reduction (ORR) and oxygen evolution reactions (OER) in Zn-air batteries[20]. The synthesis processes were impregnating Ketjenblack (KB) into a silk fiber solution followed by drying and calcination, resulting in a randomly interconnected nanoparticle structure (Figure 2a). High-resolution transmission electron microscopy (HRTEM) revealed a hybrid composition of porous, distorted graphitic, and amorphous regions within the nanocarbon (Figure 2b). X-ray photoelectron spectroscopy (XPS) analysis of the N 1s spectrum identified pyridinic and graphitic nitrogen as the dominant species, which are known to contribute significantly to ORR/OER activity (Figure 2c). Figure 2d presents the ORR performance of nanocarbon samples synthesized with varying Ketjenblack-to-silk ratios. The SilkNC/KB with an optimal ratio of silk and KB had a half-wave potential ($E_{1/2}$) of 30 mV and a current density of approximately 6 mA cm^{-2}, indicating excellent conductivity and a high density of catalytic sites. Consequently, Zn-air batteries incorporating the SilkNC/KB electrode exhibited strong cycling stability, exhibiting a voltage gap of 1.03 V and a voltaic efficiency of 51.4% after 100 cycles (Figure 2e).

 doi:10.20944/preprints202507.1731.v1

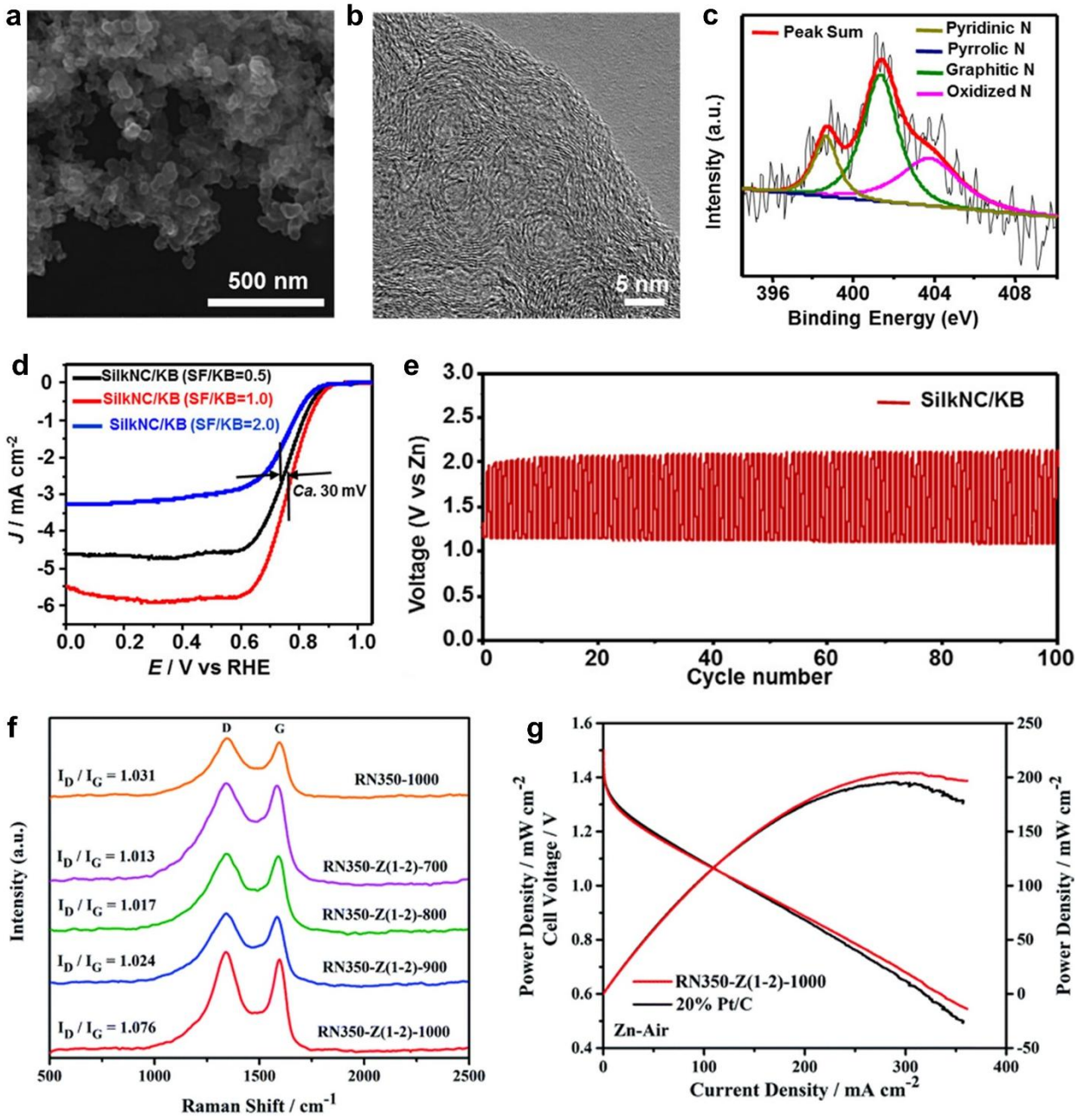

Figure 2. Protein-derived biomass carbon for the electrode for Zn-air batteries. (a) Scanning electron microscopy (SEM) image, (b) High-resolution transmission electron microscopy (HRTEM) image and (c) high-resolution X-ray photoelectron spectroscopy (XPS) spectrum of N 1s for silk-derived defect-rich and nitrogen-doped nanocarbon electrocatalyst (SilkNC/KB; silk/KB = 1.0; pyrolysis temperature = 1050 °C); (d) Electrochemical oxygen reduction reaction (ORR) and the oxygen evolution reaction (OER) performance of SilkNC/KB; (e) galvanostatic discharge–charge cycling curves of the rechargeable Zn–air batteries based on SilkNC/KB catalyst[20]. Copyright 2019, American Chemical Society. (f) Raman patterns of root-nodule-derived carbon that carbonized and pyrolysis at different temperature (RN350-1000, RN350-Z(1-2)-T; T = 700, 800, 900, 1000 °C) ; (g) Zn–air battery polarization curves and corresponding power density curves using RN350-Z(1-2)-1000 and 20% Pt/C as the cathode[21]. Copyright 2021, Royal Society of Chemistry.

In a separate study, protein-rich root nodules were transformed into effective electrocatalysts for Zn-air batteries[21]. The root nodules contain two metalloproteins, olybdenum-iron (MoFe) protein and iron (Fe) protein, which function as enzymes within the nitrogenase complex. The root nodules were carbonized and activated by $ZnCl_2$ within a temperature range of 700-1000 °C. This thermal treatment enabled the in-situ formation of a carbon-based catalyst doped with sulfur,

 doi:10.20944/preprints202507.1731.v1

nitrogen, molybdenum and iron, while simultaneously achieving a high specific surface area (SSA) and high degree of graphitization (Figure 2f). The inherent metal atoms embedded in the protein polypeptide chains promoted the uniform distribution of metal clusters within the resulting porous carbon matrix, thereby significantly improving its electrocatalytic performance (Figure 2g).

2.1.2. Protein-Derived Carbon for Electrodes of Vanadium Redox Flow Batteries

In vanadium redox flow batteries, electrochemical reactions primarily occur at the interface of electrode materials such as carbon, transition metals and noble metals. These electrochemical reactions are key to converting stored chemical energy into usable electrical power. Enhancing the efficiency of vanadium redox flow batteries requires electrodes with a three-dimensional architecture that not only facilitates efficient electrolyte circulation but also offers a high specific surface area to expand the active reaction sites. These structural features help reduce redox reaction overpotentials and boost the electrical conductivity of electrodes in batteries.

Silk protein-derived carbon fabrics (SCFs) obtained through carbonization at temperatures between 800 and 1200 °C have been explored as electrode materials for vanadium redox flow batteries (Figure 3a, b)[22]. These SCFs provided abundant nitrogen and oxygen heteroatoms that originated from the polypeptide backbone of protein, contributing to low peak potentials (ΔE_P) of approximately 164.5 mV and 164.6 mV for the catholyte and anolyte, respectively, at a scan rate of 5 mV s^{-1}. In a separate study, a twin cocoon protein (Figure 3c) underwent hydrothermal treatment (Figure 3d) followed by carbonization (600-1000 °C) to yield a nitrogen- and oxygen-doped, self-supporting carbon monolith (Figure 3e). The structure demonstrated notable electrochemical reactivity and long-term stability in vanadium redox flow batteries[23,24]. Additionally, carbon derived from a corn protein (zein) has been employed as a catalytic electrode material (Figure 3f, g). The zein-derived carbon possessed a high specific surface area enriched with oxygen-containing groups and active sites for vanadium redox reactions, facilitating enhanced electron transport and ion kinetics (Figure 3h). The superior performance of protein-derived carbon materials can be attributed to two main characteristics. One characteristic is the integrated, porous networks that offer improved conductivity, structural flexibility and permeability; the other is the defect-rich surfaces with high nitrogen and oxygen content that promote redox activity and reversibility.

 doi:10.20944/preprints202507.1731.v1

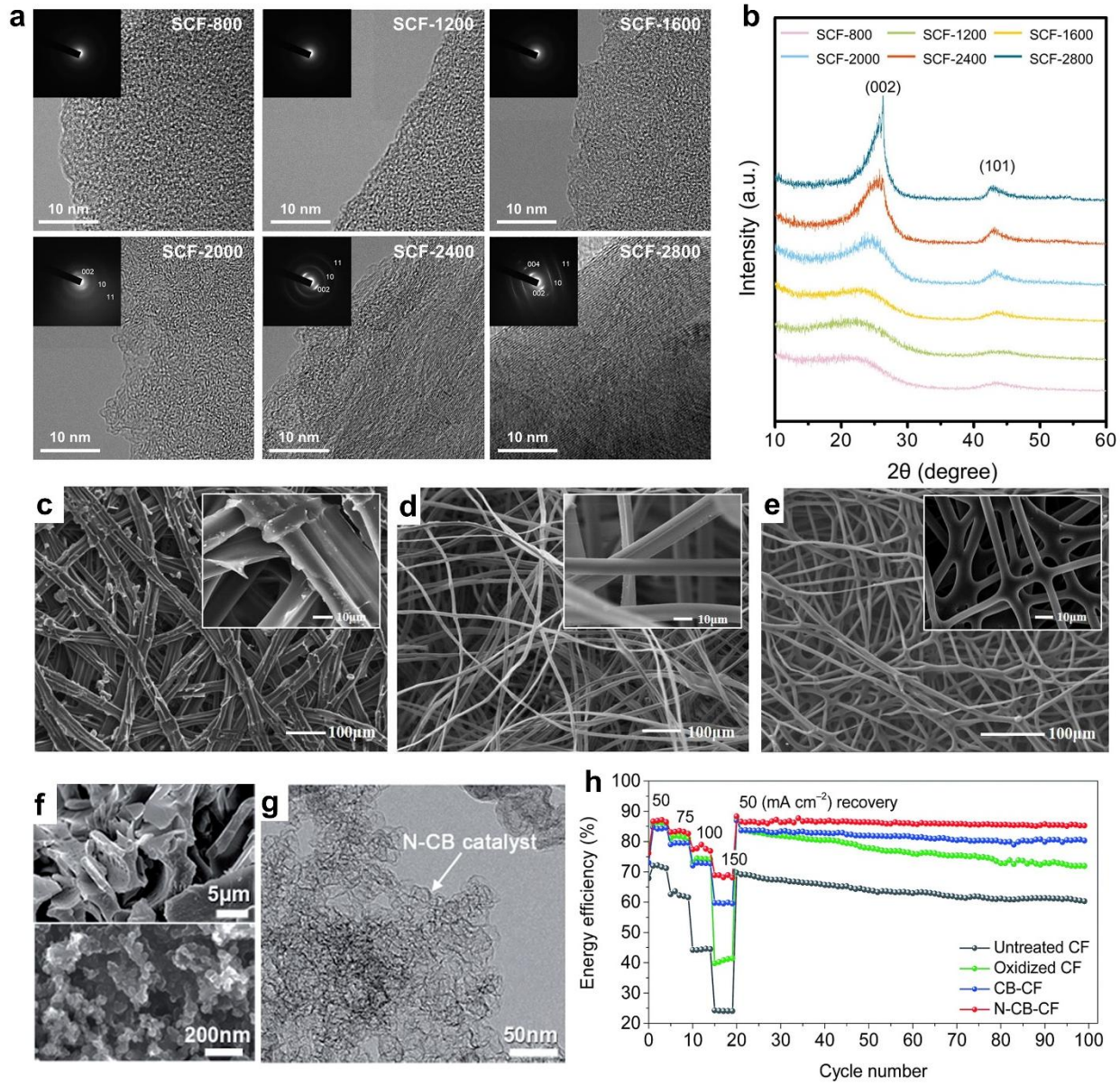

Figure 3. (a) Field emission transmission electron microscope (FETEM) images and (b) X-ray diffraction (XRD) diffractograms of the Silk protein-derived carbon fabrics (SCF-T) prepared at various calcination temperatures[22]. Copyright 2021, Elsevier. SEM images of (c) the pristine twin cocoon, (d) the hydrothermal-treated twin cocoon and (e) the carbonized twin cocoon[23]. Copyright 2019, Elsevier. (f) SEM image of pristine zein powder (upper) and the pristine carbon black (CB) nanoparticles (lower); (g) HR-TEM image of the N-CB catalyst; (h) energy efficiency of the untreated carbon felt (CF), oxidized CF, CB-CF, and N-CB-CF electrodes during the rate capability test[25]. Copyright 2021, Royal Society of Chemistry.

2.2. Protein-Modified Active Materials

Pig blood is a protein-rich biological material abundant in hemoglobin, which has been employed to synthesize an electrocatalyst featuring atomically dispersed Fe sites embedded within a two-dimensional, porous carbon matrix (**Figure 4a, b, c**)[26]. Zn salt was introduced in controlled amounts into the precursor mixture solution as an activation agent. Through strong coordination with the proteins, Zn ions formed uniformly distributed hydrolysates in the solution. After a hydrothermal treatment and pyrolysis process at 900-1000 °C within different atmosphere, a porous architecture with well-dispersed Fe-N-C active sites was obtained (**Figure 4d**). The resulting Zn-assisted Fe single-atom catalyst calcinated at 950 °C within NH_3 atmosphere (Zn/FeSA-PC/950/NH_3) contained most abundant Fe-N sites compared to other samples (**Figure 4e**). Zn/FeSA-PC/950/NH_3

 doi:10.20944/preprints202507.1731.v1

exhibited high ORR performance that characterized by a superior limiting current density along with a more positive onset potential among the samples (**Figure 4f**). Consequently, the Zn/FeSA-PC/950/NH_3 catalyst delivered a peak power density of 220 mW cm^{-2} in Zn–air batteries (ZABs) (**Figure 4g**).

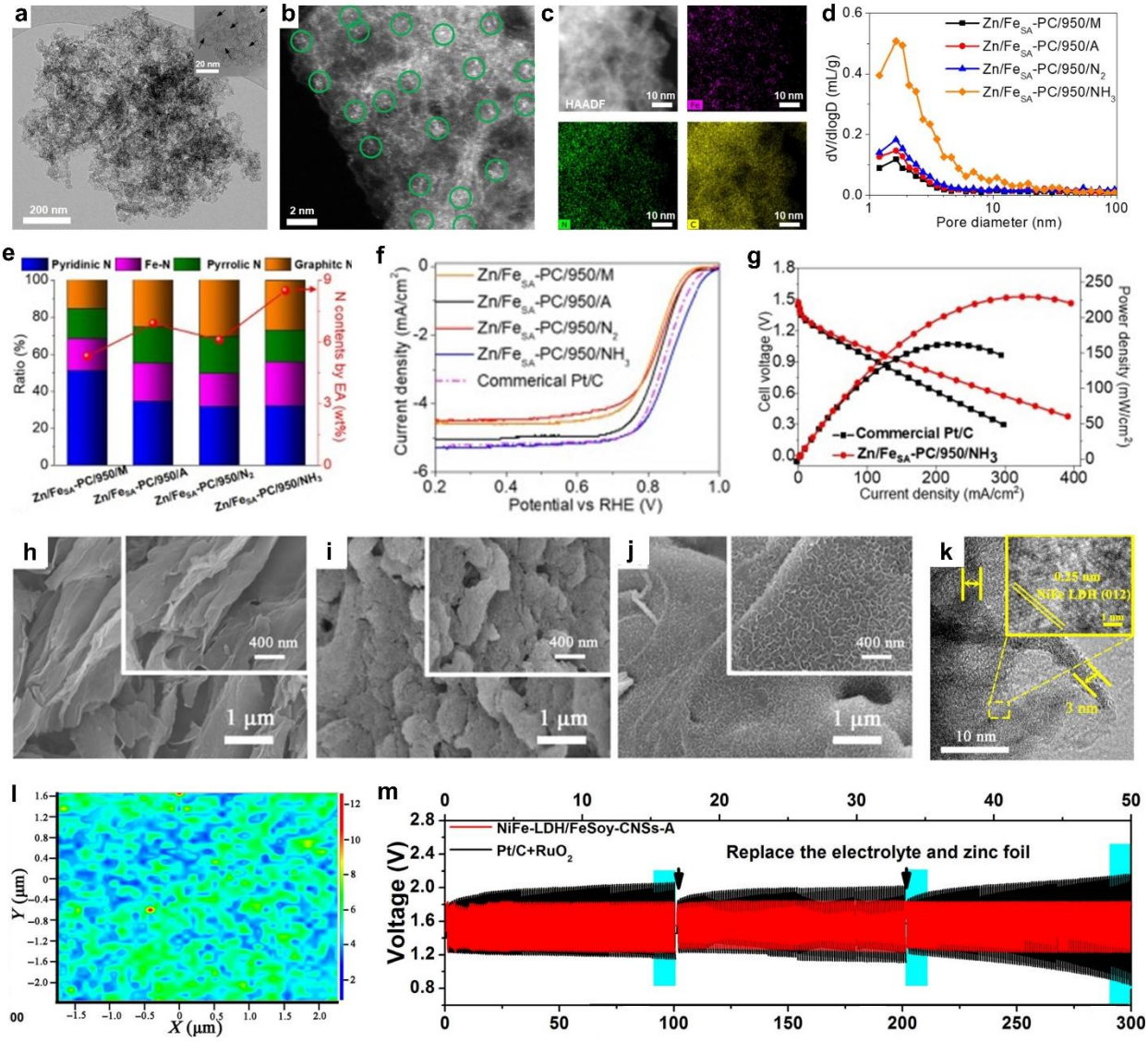

Figure 4. (a) HR-TEM image, (b) high-angle annular dark-field scanning transmission electron microscopy (HAADF-STEM) image and (c) element mapping of Zn/FeSA-PC/950/NH_3 catalyst; (d) the corresponding Barrett-Joyner-Halenda (BJH) pore size distributions; (e) the N1s according to various N groups; (f) linear sweep voltammetry (LSV) curves of Zn/FeSA-PC/950/NH_3 materials obtained in O_2-saturated 0.1 M KOH; (g) the power density plots of Zn–air batteries that used Zn/FeSA-PC/950/NH_3 catalyst and commercial Pt/C catalyst as cathode materials[26]. Copyright 2019, Elsevier. SEM images of (h) FeSoy-CNSs-A, (i) NiFe-LDH and (j) NiFe-LDH/FeSoy-CNSs-A. (k) HRTEM images of NiFe-LDH/FeSoy-CNSs-A. (i) Raman mapping of NiFe-LDH/FeSoy-CNSs-A. (m) Galvanostatic discharge-charge cycling curves using NiFe-LDH/FeSoy-CNSs-A and Pt/C+RuO_2 catalysts at 5 mA cm^{-2} with 10-min cycle[28]. Copyright 2021, Springer. .

In an earlier work, Fe-N-C framework composites were synthesized using soybeans as the carbon and nitrogen source. Soybean was mixed with $FeCl_3 \cdot 6H_2O$ via grinding and followed by a pyrolysis process to obtain the composites (**Figure 4h**)[28]. These composites served as a scaffold for the vertical growth of ultrathin NiFe-layered double hydroxide (NiFe-LDH) nanosheets (**Figure 4i**) that achieved through a simple coprecipitation process (**Figure 4j, k**). The nanosheets preferentially

 doi:10.20944/preprints202507.1731.v1

nucleated at the defect sites and oxygen-rich regions of the Fe-N-C substrate (**Figure 4l**), resulting in a composite with exceptional oxygen evolution ($E_{j=10}$ = 1.53 V vs. RHE) and oxygen reduction ($E_{1/2}$ = 0.91 V vs. RHE) reaction activity (**Table 2**). Moreover, the catalyst demonstrated impressive durability and operational stability in ZABs (**Figure 4m**).

Table 2. Protein-derived active materials for non-alkali metal-ion batteries[26–29].

Protein type	Electrode	Systems	Electrochemical performance	Separator	Electrolyte	Counter Electrode	Reference
Pig blood	2D Zn-Fe single-atom porous carbon catalyst	Zn-air AEMFCs	220 mW cm^{-2} 352 mW cm^{-2}	/ FAA-3-20 (coating toward cathode)	6.0 M KOH H_2/O_2	Zn Symmetrical gas diffusion layer	[26]
Bovine serum albumin	Protein-coated MoS_2/Gr nanosheet	Zn-air	130 W h kg^{-1}, OCV = 1.4 V	Whatman filter paper	4 M KOH	Zn	[27]
Soybean	NiFe-LDH nanowalls anchored on Fe-N-C matrix	Zn-air	OER ($E_{j=10}$ = 1.53 V vs. RHE) and ORR ($E_{1/2}$ = 0.91 V vs. RHE)	/	6.0 M KOH + 0.2 M ZnAC	Zn	[28]
Cyt c	bi-protein PQQ-GDH/cyt c signal chain	Supercapacitor /biofuel cell hybrid device	4.5 μW cm^{-2}, 80% residual activity after 50 pulses	/	Air-saturated 10 mM NaH_2PO_4	Bioanode (PQQ-GDH-cyt c-GP), biocathode (BOx-GP-cyt c)	[29]

Abbreviations: AEMFCs: Anion Exchange Membrane Fuel Cells; Whatman: glass microfiber filter; FAA-3-20: a non-reinforced anion exchange membrane; Gr: Graphene; OCV: Open circuit potential; NiFe-LDH: NiFe layered double hydroxide; OER: oxygen evolution reaction; ORR: oxygen reduction reaction; RHE: reversible hydrogen electrode. "/" indicates that the component did not exist in the related systems or was not mentioned in the literature.

In another study, bovine serum albumin (BSA), a protein in animal blood, bovine serum albumin (BSA) serves as both the exfoliating and dispersing agent, enabling the rapid production of stable hybrid suspensions in large quantities[27]. Meanwhile, a simple and one-pot top-down approach has been used to efficiently synthesize MoS_2/graphene (MoS_2/Gr) hybrid nanoplatelets in aqueous solution. In this process, the phenyl and disulfide functional groups of BSA strongly interact with MoS_2, exhibiting a binding energy of 0.51 eV that significantly higher than the interlayer binding energy of MoS_2 (0.21 eV), which facilitates effective exfoliation. When applied in zinc–air batteries, the MoS_2/Gr hybrid with a 1:13 molar ratio exhibited enhanced ORR performance, delivering a high open-circuit voltage of 1.4 V and a notable specific energy density of around 130 Wh kg^{-1}.

3. Protective Films for Zn Metal Anodes

A biomolecule-assisted approach using collagen hydrolysate (CH)-modified separator has been reported to suppress dendrite formation in Zn metal batteries[30]. The CH-coated separator, collagen hydrolysate on absorbed glass mat (CH@AGM), was prepared by dissolving CH in hot water and then uniformly coating it onto a porous AGM substrate (**Figure 5a**). The symmetrical Zn|AGM|Zn cell delivered a current of -46 mA at -0.2 V and maintained at -43 mA. Comparatively, the Zn|AGM + CH@AGM|Zn configuration shows a steadily increasing current beginning at −0.34 V (**Figure 5b**). This CH coating introduced a negatively charged surface in both aqueous electrolytes, facilitating enhanced surface conduction and ion transport regulation (**Figure 5c**). The CH molecules interact strongly with Zn^{2+} ions due to the presence of amino acid sequences (mainly glycine, proline, and hydroxyproline) capable of forming stable complexes. Moreover, anions such as SO_4^{2-} or PF_6^- were driven away by the intense electric field, which amplifies ion depletion in the bulk and triggers a "deionization shock" phenomenon (**Figure 5f**). This process promoted uniform "shock electrodeposition" behind the shock front and effectively suppressed the formation of dendrites. In

 doi:10.20944/preprints202507.1731.v1

the aqueous electrolyte containing 2% CH, the Zn coating on the anode surface appeared only partially distributed, featuring fine grains smaller than 1 μm (**Figure 5d**). In contrast, the pristine aqueous electrolyte produced a more continuous granular structure, with grain sizes reaching up to 10 μm on the anode surface (**Figure 5e**). The symmetrical Zn|AGM + CH@AGM|Zn cell demonstrates lower mass transfer-controlled potential values and improved potential retention compared to symmetrical Zn|AGM|Zn cell (**Figure 5g**). Moreover, Zn||LMO full cells with CH@AGM exhibited over 600 stable cycles at 1 C and maintaining >90% capacity retention with high-loading cathodes of 24 mAh cm^{-2} (**Figure 5h**). Even under high-temperature conditions (60°C), CH@AGM-stabilized batteries showed minimal performance degradation. The strategy was validated in large-volume batteries (5 Ah, 65 Ah, and 200 Ah Zn metal cells) that demonstrated the scalability.

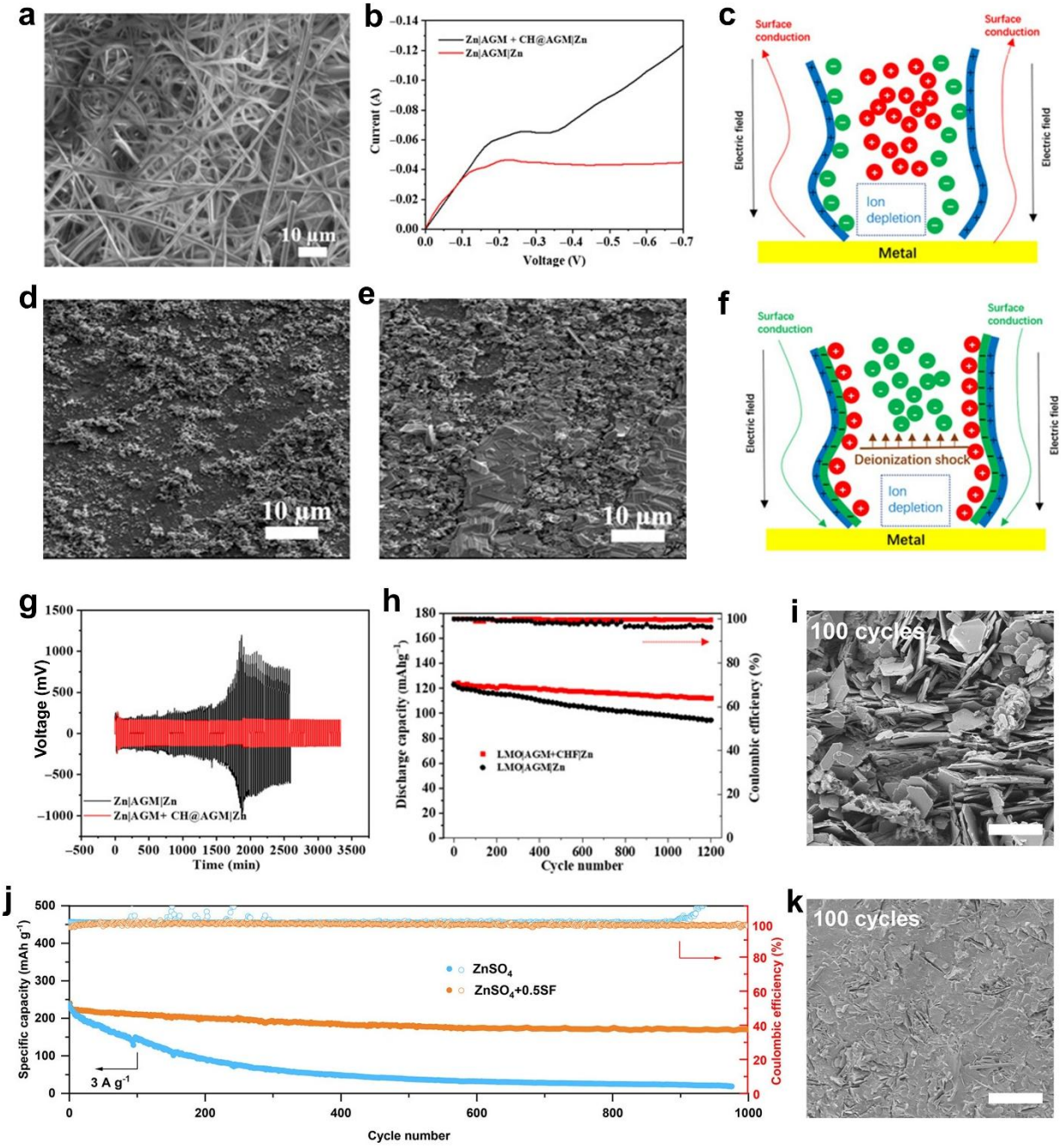

Figure 5. (a) SEM images of collagen hydrolysate coated on absorbed glass mat (CH@AGM); **(b)** Voltammetry of Zn|AGM + CH@AGM|Zn and Zn|AGM|Zn cells in the 1 M $ZnSO_4$ electrolyte at a scan rate of 1 mV s^{-1}; **(c and f)** mechanistic sketches of the effect of surface conduction on metal electrodeposition in a charged pore; SEM

 doi:10.20944/preprints202507.1731.v1

images of the Zn anode in Zn|AGM|Zn cell after 10 min of chronoamperometry **(d)** with and **(e)** without CH in the aqueous electrolyte; **(g)** galvanostatic Zn plating/stripping voltage profiles for symmetric Zn|AGM + CH@AGM|Zn and Zn|AGM|Zn cells at a capacity of 1 mAh cm^{-2} and a current density of 1 mA cm^{-2}; **(h)** cycling performance of the discharge capacity and coulombic efficiency of LMO|AGM + CH@AGM|Zn and LMO|AGM|Zn cells with the 3.6 mAh cm^{-2} cathode at a rate of 1 C[30]. Copyright 2020, American Association for the Advancement of Science. **(i)** Pure $ZnSO_4$ and **(k)** $ZnSO_4$ + 0.5SF electrolytes with 100 cycles at 1 mA cm^{-2} and 1 mAh cm^{-2}. Scale bars: 20 μm; **(j)** Cycling performance of Zn||KVO full cells in $ZnSO_4$ and $ZnSO_4$ + 0.5SF electrolytes at a high current density of 3 A g^{-1} [31]. Copyright 2022, American Chemical Society.

Zn metal anodes are suffering from the parasitic reactions on the interface of Zn/electrolyte due to the strong activity of water molecules. In a recent study, to suppress the reactions between water and Zn, silk fibroin was reported as an additive for various aqueous electrolytes with different salts ($ZnSO_4$, $Zn(CF_3SO_3)_2$ or $ZnCl_2$)[31,32]. The fibroin protein molecules have a secondary structural transformation from regular α-helices to random coils in the electrolytes, forming a $[Zn(H_2O)_4(\text{fibroin})]^{2+}$ solvation structure and weakening the hydrogen bond of water. Meanwhile, fibroin additive generated a self-healing protective film on Zn anode, regulating Zn ion deposition and alleviating dendrite growth. As shown in **Figure 5i**, Zn anodes cycled in pure $ZnSO_4$ electrolytes exhibit a rough surface morphology characterized by irregular clusters of vertically aligned 2D hexagonal flakes. In contrast, the addition of 0.5 wt% SF results in a smoother and dendrite-free surface (**Figure 5k**). Furthermore, prolonged cycling in $ZnSO_4$ alone leads to increased dendrite accumulation on the separator. As a result, the symmetrical Zn|Zn cell displayed an excellent cycling lifespan of > 500 h. The Zn||KVO full cell has a good cycling stability (capacity retention is 82.7% at 200^{th} cycles at a current density of 0.2 A g^{-1} (**Figure 5j**).

4. Protein-Based Gel State Electrolytes for Zn-Ion Batteries

Aqueous Zn-ion batteries offer superior safety compared to Li-based systems, owing to the non-toxic nature of both the Zn metal and the aqueous electrolytes[33]. Recent research has explored the use of protein-based gel electrolytes to enhance the biodegradability and biocompatibility of Zn-ion batteries. For instance, Zhou et al. developed a plasticized gelatin-silk electrolyte for Zn-ion batteries. As shown in Figure 6a, silk protein, composed of polypeptide chains rich in amino acids, presents numerous polar side groups after treatment with $CaCl_2$. These chains adopted water-soluble coil and β-sheet conformations with an unfolded structure in solution. Upon mixing gelatin into the silk solution and subsequently removing water, a plasticized film formed and gelatin chains were uniformly embedded within the silk matrix. This integration was reinforced by the robust mechanical stability imparted by the β-sheet domains of silk. When saturated with a liquid electrolyte containing 2 mol L^{-1} $ZnSO_4$ and 0.1 mol L^{-1} $MnSO_4$, the resulting gelatin–silk electrolyte exhibits excellent ionic conductivity of 5.68×10^{-3} S cm^{-1} (Figure 6b). Zn-ion batteries assembled with this electrolyte maintain a stable operating voltage of 1.55 V and demonstrate reliable cycling stability over 100 cycles (Figure 6c). Notably, the battery degrades completely into a protease solution within 45 days, highlighting its environmental sustainability.

 doi:10.20944/preprints202507.1731.v1

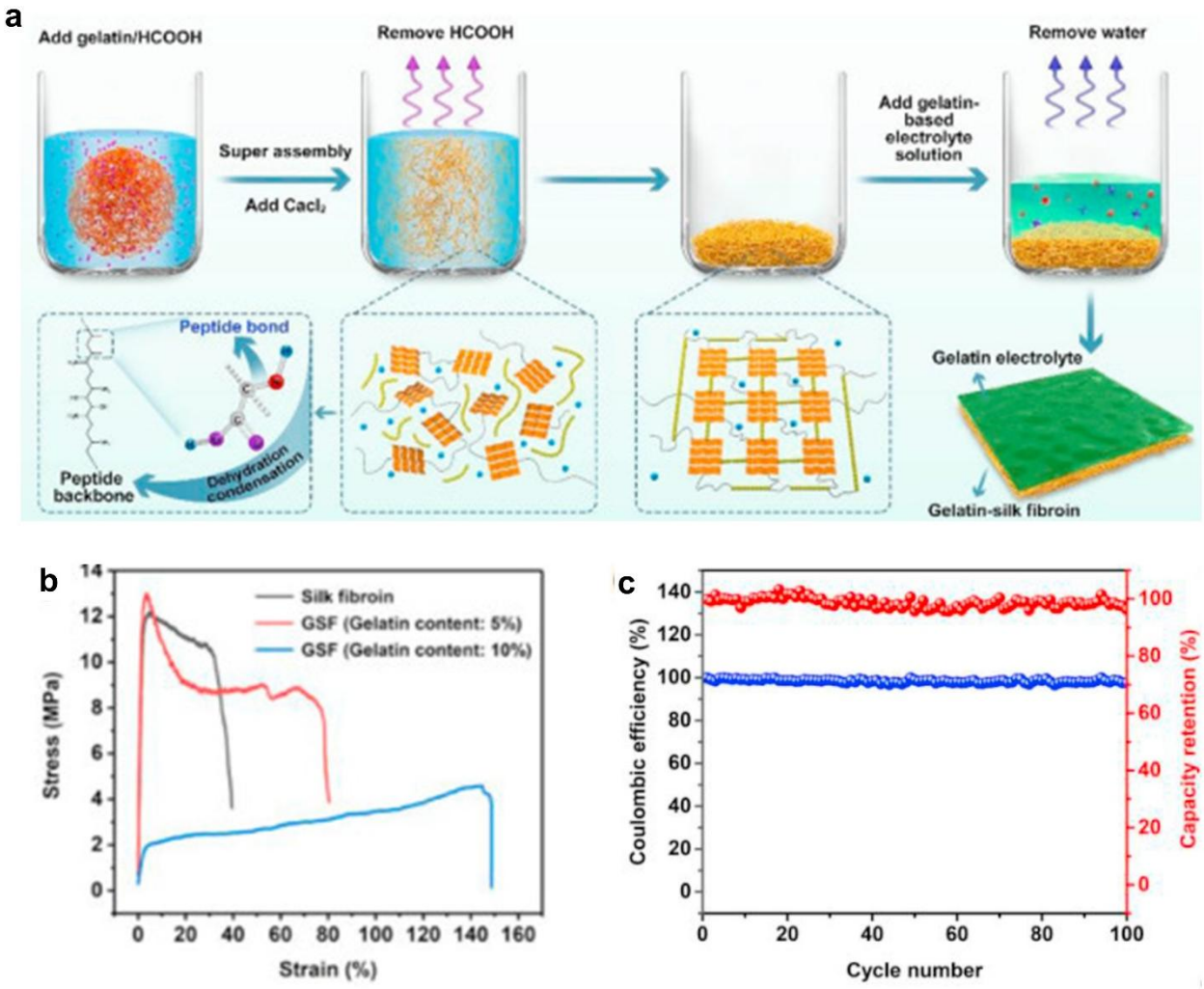

Figure 6. Gel electrolyte for Zn-ion batteries. **(a)** Schematic diagram of fabrication of gelatin-silk fibroin electrolytes; **(b)** Stress-strain curves of silk fibroin films (water content: 12%) with different gelatin weight ratios; **(c)** Long-term cycling performance and Coulombic efficiency of fiber-shaped TZIBs at 61.6 mA g^{-1} [33]. Copyright 2021, Elsevier.

5. Protein-Derived Catalysts

5.1. Biochemical Microbial Fuel Cells

Microbial fuel cells (MFCs) are promising bio-electrochemical systems for energy storage, which create the link between biologic catalytic redox activity and electrochemical reactions/physics [34,36]. The typical features of MFCs are: (1) applying bio-organisms/materials (e.g., electroactive bacteria or proteins) as the electrocatalyst in anode; (2) work temperature ranging from 15 °C and 45 °C that is in ambient levels; (3) the environmental pH is neutral; (4) using biomass materials as anodic fuel. MFCs convert the chemical energy of organic substrates to electricity by electrochemical processes (**Figure 7a**). The electron transfer mechanisms are shown in **Figure 7b**. The A spot is indirect transfer via mediators or fermentation products, the B spot is direct transfer via cytochrome proteins, and the C spot is direct transfer via conductive pili. During the process, direct electron transfer between electrode (e.g., anode) and biofilm *via* cytochrome membrane proteins (mechanism B in **Figure 7b**) is one type of electron transfer mechanism. For example, BSA with high water solubility was applied as organic matter in wastewater electrolyte for a single-chamber microbial fuel cell[35]. With optimized concentrations, MFCs with BSA (1100 mg L^{-1}) achieved a maximum power densities of ~ 354 mW m^{-2} that is higher than ~ 269 mW m^{-2} of the MFC with peptone (300 mg L^{-1}) (**Figure 7c**). Meanwhile, the CE (20.6%) of MFC with BSA is larger than that with peptone (6.0%) (**Figure 7d**). In

 doi:10.20944/preprints202507.1731.v1

recent study, various plant proteins extracted from different oil meals, were used as the low-cost, sustainable and biodegradable electrolyte (or biodiesel) for MFCs[37]. By using copper plates as symmetrical electrodes, MFC achieved an output voltage of up to 300 mV and a maximum current of ~ 9 mA when the electric resistance is 10 Ω.

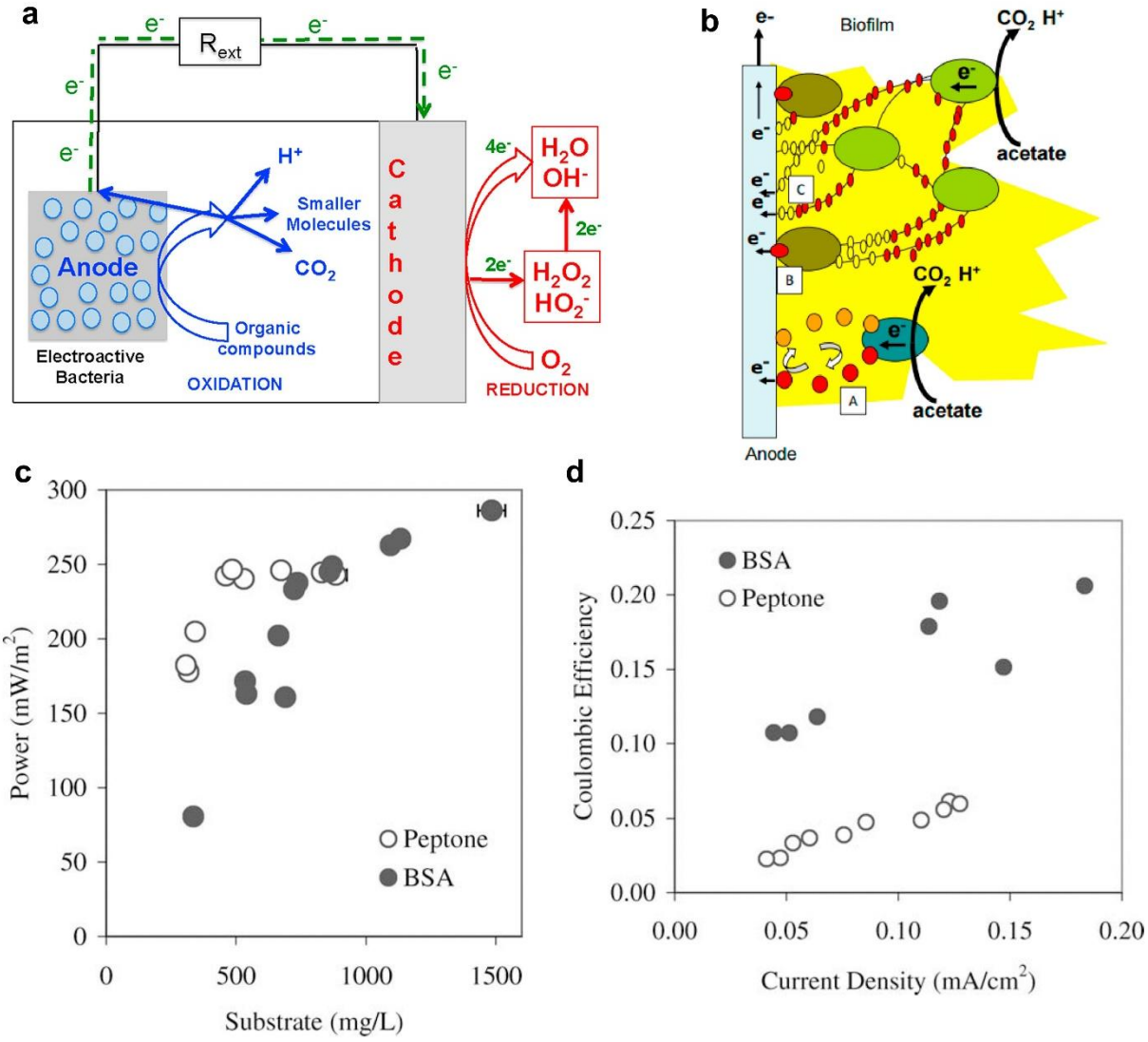

Figure 7. (a) Schematic of a microbial fuel cell; **(b)** mechanisms involved in electron transfer[34]. Copyright 2017, Elsevier. **(c)** Maximum power density with peptone or BSA as a function of substrate concentration; **(d)** Columbic efficiencies as a function of current density using BSA (1100 mg L^{-1}) and peptone (500 mg L^{-1})[35]. Copyright 2006, Wiley-VCH.

5.2. Biochemical H_2-NH_3 Systems

Nitrogenases are enzymes generated by some bacteria and are responsible for the synthesis of NH_3 from N_2. Nitrogenases, such as MoFe protein, consist of a catalytic protein and a homodimeric reducing component protein (Fe protein). Based on the biofunctions of Nitrogenases, enzymatic fuel cells (EFC: one specific MFC) were constructed by utilizing enzymes as electrocatalysts for electrochemical reactions, enabling the possible production of NH_3 at ambient temperature/pressure and near-neutral pH. However, the sluggish electron transfer between enzyme catalysts and electrodes requires the addition of reversible electron mediators. Meanwhile, good compatibility of bioanode and electron mediators is critical to the performance of EFC. To address the two issues, D. Milton et al. applied methyl viologen (N,N'-dimethyl-4,4'-bipyridinium, MV) as the only electron

 doi:10.20944/preprints202507.1731.v1

donor of the catalyst to facilitate the electrochemical reduction of C_2H_2, H^+ and N_2 [38]. It was demonstrated that MV acts as the electron mediator for bioanode (NiFe hydrogenase) and bicathode (nitrogenase), simultaneously producing electricity and NH_3 from H_2 and N_2 (**Figure 8a**). The resulting EFC not only successfully produced NH_3 with a yield amount of 286 nmol NH_3For 1 mg^{-1} MoFeprotein, but also exhibited an open circuit potential of ~ 228 mV (**Figure 8c**), maximum current of ~ 48 μA cm^{-2} (**Figure 8b**) and power density of ~ 1.5 mW cm^{-2} (**Figure 8d**).

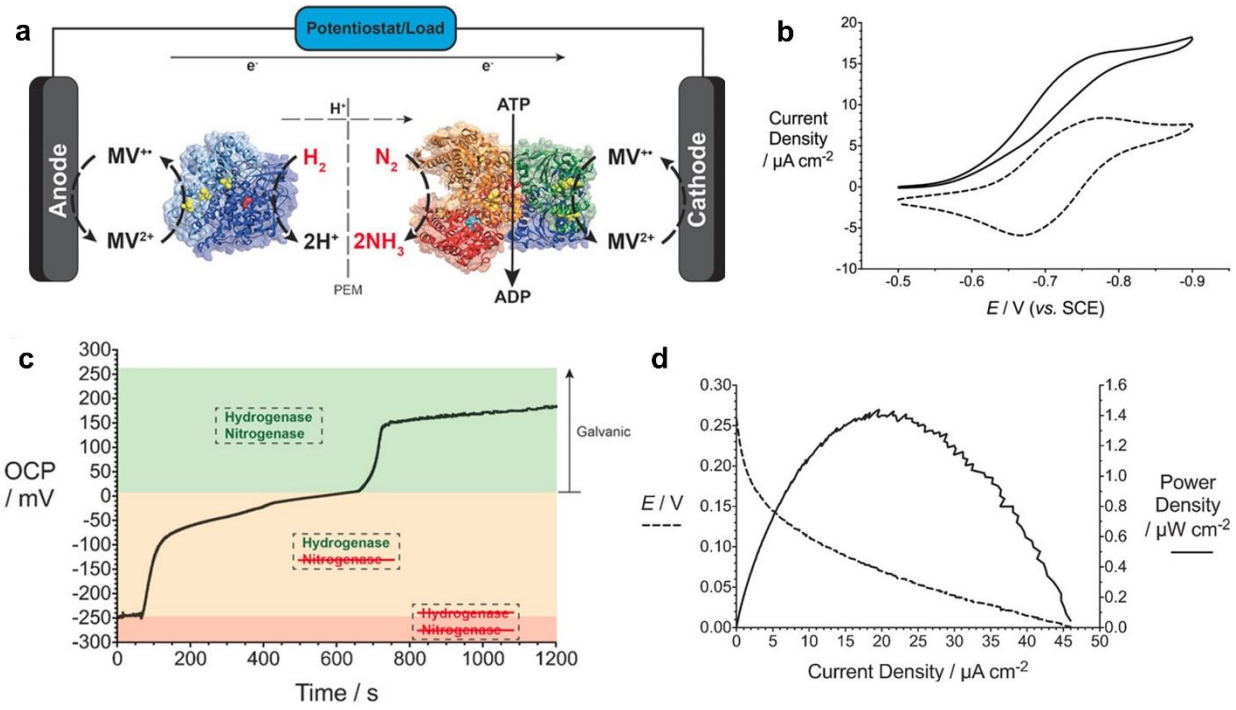

Figure 8. (a) Enzymatic fuel cell (EFC) setup using a proton exchange membrane to separate hydrogenase and nitrogenase (Fe/MoFe proteins). Methyl viologen (MV) mediates electron transfer, enabling simultaneous NH_3 and electricity production from H_2 and N_2 at room temperature and ambient pressure. **(b)** Cyclic voltammogram of N_2 reduction by nitrogenase with MV as mediator in MOPS buffer (pH=7, 100 mM), showing responses with (solid) and without (dashed) 6.7 mM $MgCl_2$. Scan rate: 2 $mV{\cdot}s^{-1}$; Toray paper electrode (0.25 cm^2). **(c)** OCP evolution of H_2/N_2 EFC. H_2/hydrogenase added at 60 s (anode); N_2/nitrogenase/MV^+ at cathode. $MgCl_2$ was added at 660 s to activate ATP hydrolysis. **(d)** Polarization and power curves from linear sweep voltammetry (0.5 $mV{\cdot}s^{-1}$)[38]. Copyright 2017, Wiley-VCH.

5.3. Bio-Nanobatteries

A nanoscale energy storage device, bio-nanobattery, was developed using ferritin protein-contained metal chemicals as electrodes[39]. Ferritin has characteristics of spherical protein shells, stability under extreme conditions, and the capability to house metal ions in its interior. Ferritins were engineered to contain Fe^{2+} as the anode material and Co^{3+} as the cathode material (**Figure 9a**). An ion-permeable membrane was placed between the ferritin-derived anode and cathode to build a compact electrochemical cell (**Figure 9b**). Upon closing the external circuit, electrons transfer from the Fe^{2+}-containing ferritin to the Co^{3+}-containing ferritin, enabling voltage generation of approximately 350-500 mV and efficient charge transfer. Cyclic voltammetry demonstrated that the ferritin electrodes showed stable redox cycling without additional mediators, highlighting the capacity for direct electron conduction from the mineral core through the protein shell to the electrode surface, which was a vital characteristic for practical nano-battery applications (**Figure 9c**). The initial discharge curve of the bio-nanobattery by time further demonstrated the successful electrochemical energy storage construction (**Figure 9d**). The ferritin-based nanobattery presents a compelling model for biocompatible, flexible and efficient energy storage on the nanoscale.

 doi:10.20944/preprints202507.1731.v1

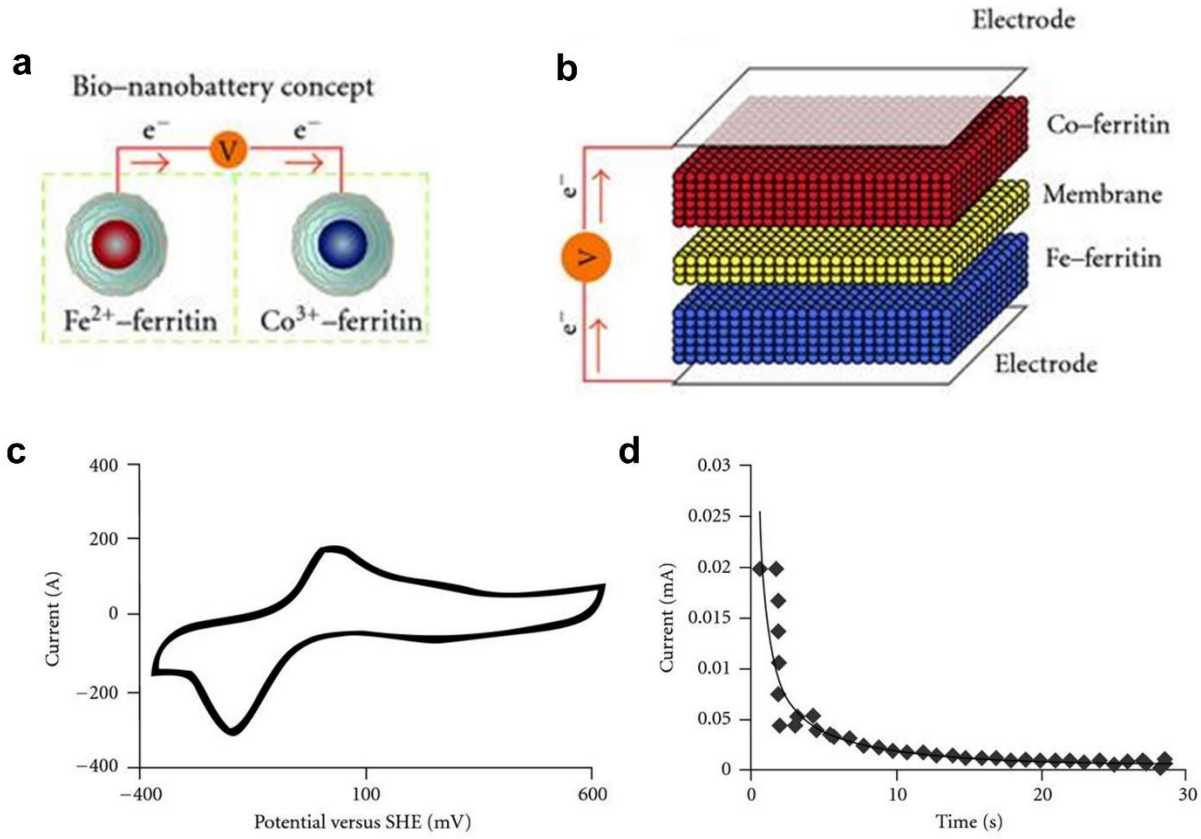

Figure 9. (a) Schematic of a bio-nanobattery using ferritin with $Fe(OH)_2$ anode and $Co(OH)_3$ cathode, immersed in 0.05 M buffer (pH 7.0-9.0, 0.10 M NaCl). **(b)** Multilayered ferritin battery with alternating charged layers (blue: anode, red: cathode); yellow membrane optional. SEM and AFM images show five ferritin layers. **(c)** Voltage cycling at 100 $mV \cdot s^{-1}$ in 0.05 M MOPS (pH=7.0) with 0.05 M thioglycolic acid (TGA). **(d)** Discharge curve of a cell with $Fe(OH)_2$ and $Co(OH_3$ ferritins on gold electrodes (pH=8.0; drain rate = 100 nA)[39]. Copyright 2012, Hindawi.

6. Polypeptide Organic Radical Batteries

Organic radical batteries are promising alternative non-alkali metal-ion batteries because of their advantages of low cost, non-containing of strategic metals and faster charge[41,42]. However, the mainstream functional organic molecules, such as 2,2,6,6-tetramethyl-4-piperidine-1-oxyl (TEMPO), in organic radical batteries are non-degradable and bring new environmental problems. To solve this issue, Nguyen et al. reported a degradable and polypeptide-based organic radical battery[40]. Polypeptide-based anode and cathode with redox-active pendant groups were prepared to build electrochemical reactions for all-polypeptide batteries. To synthesize redox-active polypeptides, L-gultamic acid (Glu), a conventional amino acid, was applied as the starting molecule to prepare the viologen-installed polypeptides for the anode and TEMPO-installed polypeptides for the cathode. The synthesis process starts from an esterification reaction (add chloro/alkynyl groups on Glu molecules) and cyclization to prepare monomer, thereafter, a polymerization followed by a grating reaction was used to synthesize the polypeptides with desired residues (**Figure 10a**). During the charging process (**Figure 10b left**), nitroxide radical functional groups (N-O· in cathode) loss electron and were oxidized to oxoammonium cations (+N=O); viologen functional groups ($Viol^{2+}$ at the anode) obtained electron and were reduced to their low valence ($Viol^{+\cdot}$) and then neutral ($Viol^0$) forms. The discharging process (**Figure 10b right)** possesses the reverse electrochemical reaction of the charging process. These electrochemical reactions were demonstrated by cyclic voltammetry test results in (**Figure 10c**). The full cells with Viol polypeptide-based anode and TEMPO polypeptide-based cathode built 44.5 mA h g^{-1} based on the amount of anode active materials and still possess electric

 doi:10.20944/preprints202507.1731.v1

storage capacity after over 200 cycles (**Figure 10d, e**). The polypeptide-based full battery also shows excellent degradability in an acid solution with an elevated temperature.

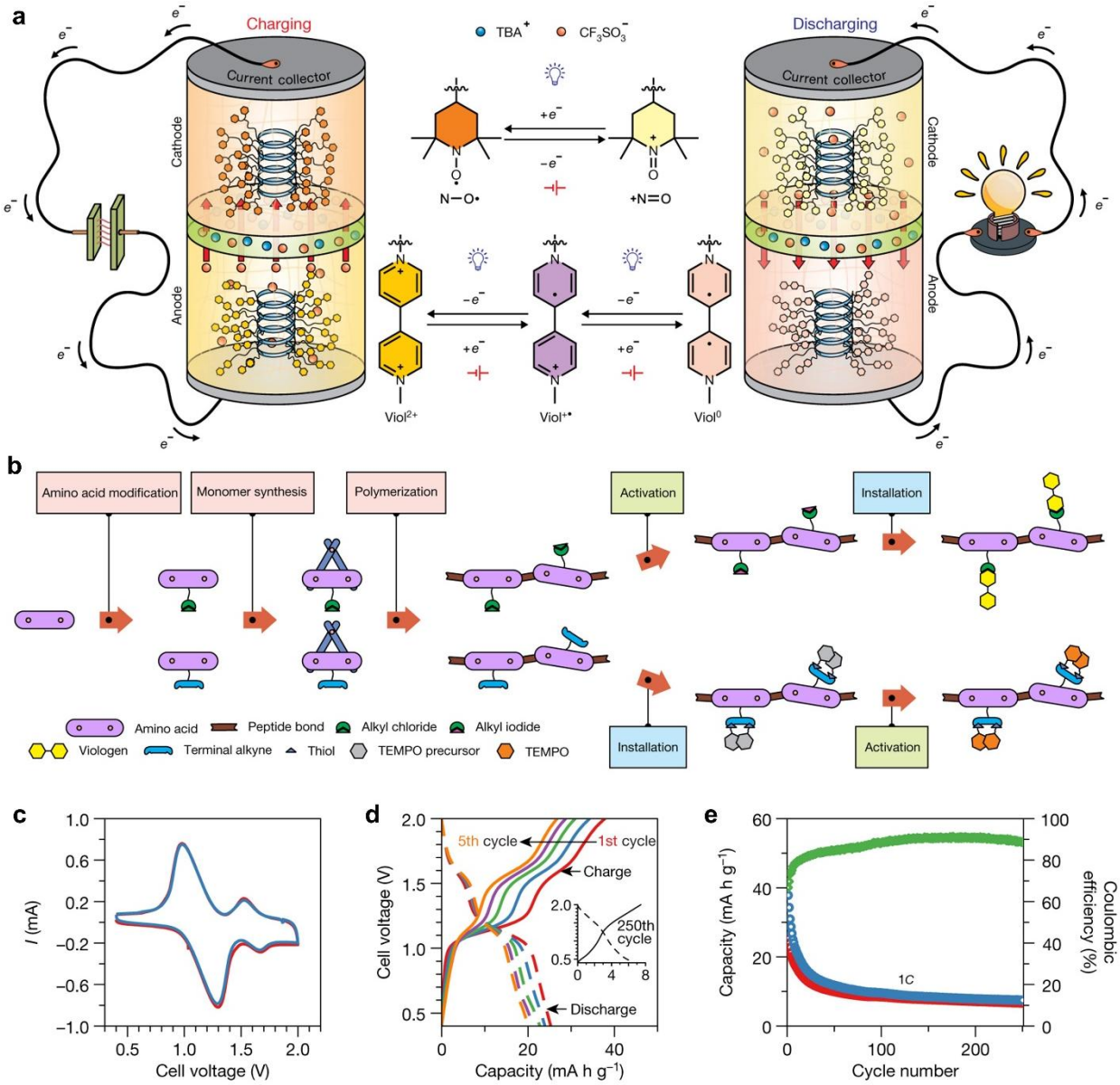

Figure 10. Polypeptide organic radical batteries[40]. (a) Schematics of a polypeptide-based organic radical battery and the reactions that occur during charging and discharging are shown on the left and right, respectively; (b) Synthesis strategy of redox-active polypeptides; (c) cyclic voltammograms, (d) charge–discharge curves solid, charge; dashed, discharge) and (e) cycling response of the viol-Cl–biTEMPO polypeptide full cell; A viol-Cl polypeptide composite electrode was separated from a biTEMPO polypeptide composite electrode by filter paper soaked in 0.5 M $TBACF_3SO_3$ in propylene carbonate. The composite electrodes were composed of 30 wt% active polypeptide, 60 wt% carbon black and 10 wt% polyvinylidene fluoride on ITO-coated glass[40]. Copyright 2020, American Association for the Advancement of Science.

7. Conclusions and Perspectives

This review comprehensively summarizes the protein-based materials and strategies applied in non-alkali metal-ion batteries that include redox flow batteries, Zn-air batteries and bio-electrochemical systems and organic radical batteries. Protein-based and protein-derived materials exhibit remarkable structural tunability, rich chemical compositions, and intrinsic biocompatibility,

 doi:10.20944/preprints202507.1731.v1

which make them excellent candidates for various components in sustainable non-alkali metal ion battery systems.

(1) Protein-derived biomass carbon materials have attracted attention for their high surface area, porous architecture, and tunable surface chemistry. The biomass carbon derived from proteins such as silk, root nodule protein and zein, has demonstrated excellent performance as electrodes in Zn-air batteries and vanadium redox flow batteries (VRFBs). In Zn-air batteries, nitrogen-doped carbon from silk and protein-rich root nodules has enabled effective oxygen reduction and evolution reactions, offering good catalytic activity and long cycling stability. In VRFBs, carbonized silk and zein-based materials exhibited improved redox kinetics and high electrochemical reversibility, which were attributed to their high nitrogen/oxygen content and interconnected conductive networks.

(2) Protein-modified active materials have improved battery performance by integrating single-atom catalysts or nanocomposites within protein-derived carbon matrices. Fe-N-C structures derived from pig blood or soybean showed enhanced ORR activity and durability in Zn-air batteries. Additionally, bovine serum albumin (BSA) was used as an exfoliation agent to synthesize MoS_2/graphene hybrids, improving their dispersion and electrocatalytic performance. The non-alkali metal ion battery systems with the protein-derived active materials demonstrated improved power densities, voltage outputs, and cycling lifespans.

(3) Proteins were able to regulate zinc metal anodes to suppress dendrite formation and side reactions with water in aqueous Zn-ion batteries. Collagen hydrolysate (CH) and silk fibroin (SF) have been successfully applied to construct protective films on Zn metal anode, leading to smoother Zn deposition that improved cycling stability even under high-temperature conditions. These protein molecules contributed to stable solvation structures and ion transport regulation, demonstrating potential scalability from coin cells to large-format batteries.

(4) Proteins also served as promising candidates in gel electrolytes for biodegradable and flexible Zn-ion batteries. A gelatin-silk protein composite formed a plasticized gel matrix with good ionic conductivity and mechanical robustness. The gel electrolyte delivered consistent voltage output and degraded in enzymatic environments, aligning with growing interest in transient and eco-friendly energy storage technologies.

(5) Proteins have been applied as catalysts and mediators in bio-electrochemical systems including microbial fuel cells (MFCs) and enzymatic fuel cells (EFCs). MFCs using protein-rich substrates like BSA or plant proteins have achieved higher power densities and coulombic efficiencies compared to conventional organic matter. Nitrogenase enzymes and hydrogenase are compartmentalized to simultaneously generate ammonia and electricity from nitrogen and hydrogen in EFCs.

(6) Ferritin-based bio-nanobatteries have been developed by employing ferritins loaded with $Fe(OH)_2$ and $Co(OH)_3$ as anode and cathode materials, respectively. These nanoscale batteries generated stable voltage and were fully regenerable. In addition, redox-active polypeptides synthesized from amino acids have been applied as active materials of anode and cathode of batteries, which offered competitive energy storage capacity and cycling stability while being fully degradable under mild acidic conditions.

In summary, this review highlights the growing versatility and functionality of protein-based materials in energy storage and conversion systems. Through pyrolysis, chemical modification, or self-assembly, proteins can be transformed into high-performance electrodes, electrocatalysts, electrolytes, separators, and protective films. Their natural abundance, biodegradability, and structural diversity make them attractive for building low-cost, sustainable and green non-alkali metal ion battery technologies.

Acknowledgments: This work was supported by USDA NIFA 2022-67021-38685.

References

 doi:10.20944/preprints202507.1731.v1

1. Hassan, Q.; Viktor, P.; J. Al-Musawi, T.; Mahmood Ali, B.; Algburi, S.; Alzoubi, H. M.; Khudhair Al-Jiboory, A.; Zuhair Sameen, A.; Salman, H. M.; Jaszczur, M. The Renewable Energy Role in the Global Energy Transformations. *Renew. Energy Focus* **2024**, *48* (January), 100545. https://doi.org/10.1016/j.ref.2024.100545.
2. Elalfy, D. A.; Gouda, E.; Kotb, M. F.; Bureš, V.; Sedhom, B. E. Comprehensive Review of Energy Storage Systems Technologies, Objectives, Challenges, and Future Trends. *Energy Strateg. Rev.* **2024**, *54* (June). https://doi.org/10.1016/j.esr.2024.101482.
3. Li, M.; Lu, J.; Chen, Z.; Amine, K. 30 Years of Lithium-Ion Batteries. *Adv. Mater.* **2018**, *30* (33), 1–24. https://doi.org/10.1002/adma.201800561.
4. Zampardi, G.; La Mantia, F. Open Challenges and Good Experimental Practices in the Research Field of Aqueous Zn-Ion Batteries. *Nat. Commun.* **2022**, *13* (1), 1–5. https://doi.org/10.1038/s41467-022-28381-x.
5. Leong, K. W.; Wang, Y.; Ni, M.; Pan, W.; Luo, S.; Leung, D. Y. C. Rechargeable Zn-Air Batteries: Recent Trends and Future Perspectives. *Renew. Sustain. Energy Rev.* **2022**, *154* (October 2021), 111771. https://doi.org/10.1016/j.rser.2021.111771.
6. Yao, Y.; Lei, J.; Shi, Y.; Ai, F.; Lu, Y. C. Assessment Methods and Performance Metrics for Redox Flow Batteries. *Nat. Energy* **2021**, *6* (6), 582–588. https://doi.org/10.1038/s41560-020-00772-8.
7. Liu, L.; Solin, N.; Inganäs, O. Bio Based Batteries. *Adv. Energy Mater.* **2021**, *11* (43), 1–12. https://doi.org/10.1002/aenm.202003713.
8. Tang, L.; Peng, H.; Kang, J.; Chen, H.; Zhang, M.; Liu, Y.; Kim, D. H.; Liu, Y.; Lin, Z. Zn-Based Batteries for Sustainable Energy Storage: Strategies and Mechanisms. *Chem. Soc. Rev.* **2024**, *53* (10), 4877–4925. https://doi.org/10.1039/d3cs00295k.
9. Sánchez-Díez, E.; Ventosa, E.; Guarnieri, M.; Trovò, A.; Flox, C.; Marcilla, R.; Soavi, F.; Mazur, P.; Aranzabe, E.; Ferret, R. Redox Flow Batteries: Status and Perspective towards Sustainable Stationary Energy Storage. *J. Power Sources* **2021**, *481*. https://doi.org/10.1016/j.jpowsour.2020.228804.
10. Wang, C.; Fu, X.; Ying, C.; Liu, J.; Zhong, W. Natural Protein as Novel Additive of a Commercial Electrolyte for Long-Cycling Lithium Metal Batteries. *Chem. Eng. J.* **2022**, *437* (P1), 135283. https://doi.org/10.1016/j.cej.2022.135283.
11. Wang, C.; Fu, X.; Lin, S.; Liu, J.; Zhong, W. H. A Protein-Enabled Protective Film with Functions of Self-Adapting and Anion-Anchoring for Stabilizing Lithium-Metal Batteries. *J. Energy Chem.* **2021**, *64*, 485–495. https://doi.org/10.1016/j.jechem.2021.05.014.
12. Wang, C.; Odstrcil, R.; Liu, J.; Zhong, W. H. Protein-Modified SEI Formation and Evolution in Li Metal Batteries. *J. Energy Chem.* **2022**, *73*, 248–258. https://doi.org/10.1016/j.jechem.2022.06.017.
13. Wang, C.; Zhong, W.-H. Introduction. In *Natural Protein-based Strategies for Batteries*; WORLD SCIENTIFIC, 2023; pp 1–21. https://doi.org/doi:10.1142/9789811283857_0001.
14. Wang, Y.; Xu, Y.; Zhou, J.; Wang, C.; Zhang, W.; Li, Z.; Guo, F.; Chen, H.; Zhang, H. Highly Dispersed SnO2 Nanoparticles Confined on Xylem Fiber-Derived Carbon Frameworks as Anodes for Lithium-Ion Batteries. **2020**, *879*, 114753. https://doi.org/10.1016/j.jelechem.2020.114753.
15. Wang, C.; Zhong, W. Promising Sustainable Technology for Energy Storage Devices : Natural Protein-Derived Active Materials. *Electrochim. Acta* **2023**, *441* (September 2022), 141860. https://doi.org/10.1016/j.electacta.2023.141860.
16. Wang, C.; Ren, L.; Ying, C.; Shang, J.; Mccloy, J.; Liu, J. Soy Protein as a Dual-Functional Bridge Enabling High Performance Solid Electrolyte for Li Metal Batteries. *J. Power Sources* **2024**, *620* (May), 235260. https://doi.org/10.1016/j.jpowsour.2024.235260.
17. Wang, C.; Ren, L.; Ying, C.; Liu, J.; Zhong, W. H. An Amino Acid-Enabled Separator for Effective Stabilization of Li Anodes. *ACS Appl. Mater. Interfaces* **2024**, *16* (12), 15632–15639. https://doi.org/10.1021/acsami.4c01256.
18. Wang, C.; Yang, X.; Zheng, M.; Xu, Y. Synthesis of β-FeOOH Nanorods Adhered to Pine-Biomass Carbon as a Low-Cost Anode Material for Li-Ion Batteries. *J. Alloys Compd.* **2019**, *794*, 569–575. https://doi.org/10.1016/j.jallcom.2019.04.074.
19. Sun, Y.; Shi, X. L.; Yang, Y. L.; Suo, G.; Zhang, L.; Lu, S.; Chen, Z. G. Biomass-Derived Carbon for High-Performance Batteries: From Structure to Properties. *Adv. Funct. Mater.* **2022**, *32* (24). https://doi.org/10.1002/adfm.202201584.

 doi:10.20944/preprints202507.1731.v1

20. Wang, C.; Xie, N. H.; Zhang, Y.; Huang, Z.; Xia, K.; Wang, H.; Guo, S.; Xu, B. Q.; Zhang, Y. Silk-Derived Highly Active Oxygen Electrocatalysts for Flexible and Rechargeable Zn-Air Batteries. *Chem. Mater.* **2019**, *31* (3), 1023–1029. https://doi.org/10.1021/acs.chemmater.8b04572.
21. Hao, M.; Dun, R.; Su, Y.; He, L.; Ning, F.; Zhou, X.; Li, W. In Situ Self-Doped Biomass-Derived Porous Carbon as an Excellent Oxygen Reduction Electrocatalyst for Fuel Cells and Metal-Air Batteries. *J. Mater. Chem. A* **2021**, *9* (25), 14331–14343. https://doi.org/10.1039/d1ta01417j.
22. Lee, M. E.; Jang, D.; Lee, S.; Yoo, J.; Choi, J.; Jin, H. J.; Lee, S.; Cho, S. Y. Silk Protein-Derived Carbon Fabric as an Electrode with High Electro-Catalytic Activity for All-Vanadium Redox Flow Batteries. *Appl. Surf. Sci.* **2021**, *567* (May), 150810. https://doi.org/10.1016/j.apsusc.2021.150810.
23. Wang, R.; Li, Y. Twin-Cocoon-Derived Self-Standing Nitrogen-Oxygen-Rich Monolithic Carbon Material as the Cost-Effective Electrode for Redox Flow Batteries. *J. Power Sources* **2019**, *421* (March), 139–146. https://doi.org/10.1016/j.jpowsour.2019.03.023.
24. Lee, M. E.; Jin, H. J.; Yun, Y. S. Synergistic Catalytic Effects of Oxygen and Nitrogen Functional Groups on Active Carbon Electrodes for All-Vanadium Redox Flow Batteries. *RSC Adv.* **2017**, *7* (68), 43227–43232. https://doi.org/10.1039/c7ra08334c.
25. Park, M.; Ryu, J.; Kim, Y.; Cho, J. Corn Protein-Derived Nitrogen-Doped Carbon Materials with Oxygen-Rich Functional Groups: A Highly Efficient Electrocatalyst for All-Vanadium Redox Flow Batteries. *Energy Environ. Sci.* **2014**, *7* (11), 3727–3735. https://doi.org/10.1039/c4ee02123a.
26. Kim, H. S.; Lee, J.; Jang, J. H.; Jin, H.; Paidi, V. K.; Lee, S. H.; Lee, K. S.; Kim, P.; Yoo, S. J. Waste Pig Blood-Derived 2D Fe Single-Atom Porous Carbon as an Efficient Electrocatalyst for Zinc–Air Batteries and AEMFCs. *Appl. Surf. Sci.* **2021**, *563* (May), 150208. https://doi.org/10.1016/j.apsusc.2021.150208.
27. Puglia, M. K.; Malhotra, M.; Chivukula, A.; Kumar, C. V. "simple-Stir" Heterolayered MoS2/Graphene Nanosheets for Zn-Air Batteries. *ACS Appl. Nano Mater.* **2021**, *4* (10), 10389–10398. https://doi.org/10.1021/acsanm.1c01792.
28. Zhang, M.; Zhang, J.; Ran, S.; Qiu, L.; Sun, W.; Yu, Y.; Chen, J.; Zhu, Z. A Robust Bifunctional Catalyst for Rechargeable Zn-Air Batteries: Ultrathin NiFe-LDH Nanowalls Vertically Anchored on Soybean-Derived Fe-N-C Matrix. *Nano Res.* **2021**, *14* (4), 1175–1186. https://doi.org/10.1007/s12274-020-3168-z.
29. Shen, F.; Pankratov, D.; Pankratova, G.; Toscano, M. D.; Zhang, J.; Ulstrup, J.; Chi, Q.; Gorton, L. Supercapacitor/Biofuel Cell Hybrid Device Employing Biomolecules for Energy Conversion and Charge Storage. *Bioelectrochemistry* **2019**, *128*, 94–99. https://doi.org/10.1016/j.bioelechem.2019.03.009.
30. Zhi, J.; Li, S.; Han, M.; Chen, P. Biomolecule-Guided Cation Regulation for Dendrite-Free Metal Anodes. *Sci. Adv.* **2020**, *6* (32), 1–15. https://doi.org/10.1126/sciadv.abb1342.
31. Xu, J.; Lv, W.; Yang, W.; Jin, Y.; Jin, Q.; Sun, B.; Zhang, Z.; Wang, T.; Zheng, L.; Shi, X.; Sun, B.; Wang, G. In Situ Construction of Protective Films on Zn Metal Anodes via Natural Protein Additives Enabling High-Performance Zinc Ion Batteries. *ACS Nano* **2022**, *16* (7), 11392–11404. https://doi.org/10.1021/acsnano.2c05285.
32. Zhu, M.; Ran, Q.; Huang, H.; Xie, Y.; Zhong, M.; Lu, G.; Bai, F.-Q.; Lang, X.-Y.; Jia, X.; Chao, D. Interface Reversible Electric Field Regulated by Amphoteric Charged Protein-Based Coating Toward High-Rate and Robust Zn Anode. *Nano-Micro Lett.* **2022**, *14* (1), 1–14. https://doi.org/10.1007/s40820-022-00969-4.
33. Zhou, J.; Li, Y.; Xie, L.; Xu, R.; Zhang, R.; Gao, M.; Tian, W.; Li, D.; Qiao, L.; Wang, T.; Cao, J.; Wang, D.; Hou, Y.; Fu, W.; Yang, B.; Zeng, J.; Chen, P.; Liang, K.; Kong, B. Humidity-Sensitive, Shape-Controllable, and Transient Zinc-Ion Batteries Based on Plasticizing Gelatin-Silk Protein Electrolytes. *Mater. Today Energy* **2021**, *21*. https://doi.org/10.1016/j.mtener.2021.100712.
34. Santoro, C.; Arbizzani, C.; Erable, B.; Ieropoulos, I. Microbial Fuel Cells: From Fundamentals to Applications. A Review. *J. Power Sources* **2017**, *356*, 225–244. https://doi.org/10.1016/J.JPOWSOUR.2017.03.109.
35. Heilmann, J.; Logan, B. E. Production of Electricity from Proteins Using a Microbial Fuel Cell. *Water Environ. Res.* **2006**, *78* (5), 531–537. https://doi.org/10.2175/106143005X73046.
36. Kannan, A. M.; Renugopalakrishnan, V.; Filipek, S.; Li, P.; Audette, G. F.; Munukutla, L. Bio-Batteries and Bio-Fuel Cells: Leveraging on Electronic Charge Transfer Proteins. *J. Nanosci. Nanotechnol.* **2009**, *9* (3), 1665–1678. https://doi.org/10.1166/jnn.2009.SI03.
37. Venkatesha, B.; Guna, V.; Bhuvaneswari, H. B.; Reddy, N. A Study on the Potential of Using Plant Proteins as Electrolytes in a Biochemical Cell. *Environ. Prog. Sustain. Energy* **2018**, *37* (3), 961–967. https://doi.org/10.1002/ep.12753.

 doi:10.20944/preprints202507.1731.v1

38. Milton, R. D.; Cai, R.; Abdellaoui, S.; Leech, D.; De Lacey, A. L.; Pita, M.; Minteer, S. D. Bioelectrochemical Haber–Bosch Process: An Ammonia-Producing H2/N2Fuel Cell. *Angew. Chemie - Int. Ed.* **2017**, *56* (10), 2680–2683. https://doi.org/10.1002/anie.201612500.
39. Watt, G. D.; Kim, J. W.; Zhang, B.; Miller, T.; Harb, J. N.; Davis, R. C.; Choi, S. H. A Protein-Based Ferritin Bio-Nanobattery. *J. Nanotechnol.* **2012**, *2012*. https://doi.org/10.1155/2012/516309.
40. Nguyen, T. P.; Easley, A. D.; Kang, N.; Khan, S.; Lim, S. M.; Rezenom, Y. H.; Wang, S.; Tran, D. K.; Fan, J.; Letteri, R. A.; He, X.; Su, L.; Yu, C. H.; Lutkenhaus, J. L.; Wooley, K. L. Polypeptide Organic Radical Batteries. *Nature* **2021**, *593* (7857), 61–66. https://doi.org/10.1038/s41586-021-03399-1.
41. Janoschka, T.; Hager, M. D.; Schubert, U. S. Powering up the Future: Radical Polymers for Battery Applications. *Adv. Mater.* **2012**, *24* (48), 6397–6409. https://doi.org/10.1002/adma.201203119.
42. Zhang, K.; Monteiro, M. J.; Jia, Z. Stable Organic Radical Polymers: Synthesis and Applications. *Polymer Chemistry*. The Royal Society of Chemistry September 13, 2016, pp 5589–5614. https://doi.org/10.1039/c6py00996d.